Theor Chem Acc (2011) 130:711–724
DOI 10.1007/s00214-010-0871-y

REGULAR ARTICLE

(Hyper)polarizability density analysis for open-shell molecular systems based on natural orbitals and occupation numbers

Masayoshi Nakano · Hitoshi Fukui · Takuya Minami · Kyohei Yoneda · Yasuteru Shigeta · Ryohei Kishi · Benoît Champagne · Edith Botek · Takashi Kubo · Koji Ohta · Kenji Kamada

Received: 13 August 2010 / Accepted: 1 December 2010 / Published online: 13 January 2011

Abstract We have developed a method for analyzing the (hyper)polarizabilities of open-shell molecular systems. This method employs the (hyper)polarizability densities based on the natural orbitals and occupation numbers, which enables us to analyze the contributions of odd electrons having various open-shell (diradical) characters. Within broken-symmetry, i.e., spin-unrestricted, single-determinant molecular orbital and density functional theory approaches, we can also remove the spin contamination effects on these quantities through spin projection. To do that, an approximate spin projected method has been elaborated and applied to the analysis of the (hyper)polarizability of multi-radical systems. As examples, typical open-shell singlet systems, 1,3-dipoles and rectangular graphene nanoflakes, are examined.

Keywords Hyperpolarizability · Open-shell molecule · Diradical · Natural orbital · Broken-symmetry method · Spin projection

Dedicated to Professor Akira Imamura on the occasion of his 77th birthday and published as part of the Imamura Festschrift Issue.

M. Nakano (✉) · H. Fukui · T. Minami · K. Yoneda · Y. Shigeta · R. Kishi
Department of Materials Engineering Science, Graduate School of Engineering Science, Osaka University, Toyonaka, Osaka 560-8531, Japan
e-mail: mnaka@cheng.es.osaka-u.ac.jp

B. Champagne · E. Botek
Laboratoire de Chimie Théorique, Facultés Universitaires Notre-Dame de la Paix (FUNDP), rue de Bruxelles, 61, 5000 Namur, Belgium
e-mail: benoit.champagne@fundp.ac.be

T. Kubo
Department of Chemistry, Graduate School of Science, Osaka University, Toyonaka, Osaka 560-0043, Japan
e-mail: kubo@chem.sci.osaka-u.ac.jp

K. Ohta · K. Kamada
Research Institute for Ubiquitous Energy Devices, National Institute of Advanced Industrial Science and Technology (AIST), Ikeda, Osaka 563-8577, Japan
e-mail: k.ohta@aist.go.jp

K. Kamada
e-mail: k.kamada@aist.go.jp

1 Introduction

Open-shell singlet molecular systems have attracted much attention in the past few decades due to their unique chemical and physical properties [1–4], including specific reactivities [5–9]. These compounds encompass inorganic four-membered heterocyclic compounds [10, 11], efficient singlet fission chromophores for dye-sensitized solar cells [12], the Fe(dipyrazolpyridine)$_2$ system exhibiting light-induced excited spin state trapping (LIESST) [13], open-shell singlet oligoacenes [14–19], as well as nanographenes and related structures [20–30]. In addition, several synthesis strategies have been developed to design diradicals and multi-radicals with tailored spin multiplicity and open-shell character, including polynitrenes and nitreno-radicals [31, 32], spiro-fused oligo(triarylamine)s [33], diarylethene with nitronyl nitroxide radicals [34], aminyl diradicals [35], diarylnitroxide diradicals [36], and compounds built from the verdazyl radical moiety [37]. It was also found that intra- and intermolecular covalent bonds coexist in the solid state due to the open-shell character of the constituent molecules [38–41]. The nonlinear optical properties are also remarkable and have been the topic of numerous investigations. In particular, the third-order nonlinear

optical response, which is described at the molecular level by the second hyperpolarizability γ, is theoretically predicted to exhibit a strong dependence on the open-shell character, e.g., diradical character y ($0 \leq y \leq 1$) [41]: for systems having similar effective diradical distances and Coulomb repulsions, γ first increases with y, attains a maximum, and then decreases [42–44]. This behavior has been exemplified using ab initio molecular orbital (MO) and density functional theory (DFT) calculations on several diradical systems, e.g., the H_2 dissociation model [42], the *p*-quinodimethane (PQM) model [42], diphenalenyl molecules [45, 46], transition metal complexes [47, 48], and graphene nanoflakes [49]. It has been further substantiated by the measurement of large two-photon absorption cross sections in diphenalenyl diradicaloids [50] and by their theoretical interpretation [51]. These large responses have been analyzed by considering the γ density [52], which can elucidate the spatial electronic contributions to γ. Within broken-symmetry (BS), i.e., spin-unrestricted (U), ab initio MO and DFT approaches, the γ enhancement for intermediate diradical characters has been shown to originate from the field-induced charge transfer between up and down spin density distributions. Other contributions have addressed the dynamic response of the pyrrole radical [53] as well as of radical ion pair salts [54].

In addition, recent computational investigations have predicted the existence of multi-radical characters in open-shell singlet systems, e.g., large polyacenes [17, 18] and graphene nanoflakes [20, 22–27] as well as aggregates composed of diradical molecules [29]. So, a diradical character y_i is associated with each pair of $\{(\text{HONO}) - i, (\text{LUNO}) + i\}$, where $i = 0, 1, \ldots$, HONO stands for the highest occupied natural orbital and LUNO for the lowest unoccupied natural orbital. Unfortunately, the conventional analysis using the spin density and γ density distributions cannot directly clarify the contributions of unpaired electrons, i.e., odd electrons [55–57], in systems having multi-radical character. Furthermore, the removal of spin contaminations associated with the BS schemes is known to be often essential for reproducing reliable molecular structures and magnetic properties [41, 58, 59].

Therefore, in this study, we first develop within the odd electron density scheme a method for partitioning the (hyper)polarizability into the contributions of each diradical character. Then, in the BS single-determinant scheme, the spin contamination effects on the electron and (hyper)polarizability densities are approximately removed by using the spin projected occupation numbers [41, 60] and natural orbitals (NOs). In order to evaluate the applicability and the usefulness of the present method, typical open-shell singlet systems, i.e., 1,3-dipoles [61] and rectangular graphene nanoflakes [20], are examined employing spin-unrestricted (U) DFT with the long-range corrected (LC) exchange–correlation functional LC-UBLYP [62–65]. In the LC-UBLYP functional, the electron repulsion operator ($1/r_{12}$) is split into long-range (LR) and short-range (SR) electron–electron interactions via the use of a range separating parameter μ in the standard error function,

$$\frac{1}{r_{12}} = \frac{1 - \mathrm{erf}(\mu r_{12})}{r_{12}} + \frac{\mathrm{erf}(\mu r_{12})}{r_{12}}, \tag{1}$$

the first term (SR interaction) is described by a modified conventional DFT exchange functional, while the second term (LR interaction) is handled by the exact Hartree–Fock (HF) exchange. In addition, an extension to the dynamic (hyper)polarizability density as well as to the dynamic odd electron density is proposed. The (hyper)polarizability density analysis based on the NOs and occupation numbers opens a path not only to the evaluation of the multi-radical character effects on the static (non)linear optical responses or to the removal of the spin contamination effects in BS single-determinant results, but also to the analysis of the dynamics of the (non)linear optical response densities. The present method of calculation and analysis of the one-electron reduced density as well as of the (non)linear optical responses could be applicable to any one-electron property of open-shell multi-radical systems.

This paper is dedicated to Prof. Akira Imamura on the occasion of his 77th birthday, paying homage to his many contributions in quantum chemistry, molecular biophysics, and theoretical chemistry and physics.

2 Methodology

2.1 Odd electron density and diradical character

So far, two kinds of measures of the effective density and of the number of odd electrons have been proposed: one by Takatsuka et al. [55, 56] and the other by Head-Gordon [57]. These measures are useful for obtaining intuitive and pictorial descriptions of odd electron distributions as well as of radical and diradical characters in open-shell molecular systems though, in principle, these measures can be arbitrarily defined. In this subsection, we briefly review the representation of the odd electron density and the definition of the diradical character as a preparation for presentation of the partitioning scheme of the (hyper)polarizability density explained in the next subsection.

According to Head-Gordon [57], the odd electron density associated with the kth ($k = 1, \ldots, M$) NO $\phi_k(\boldsymbol{r})$ of occupation number n_k is defined by

$$D_k^{\mathrm{odd}}(\boldsymbol{r}) = \min(2 - n_k, n_k)\phi_k^*(\boldsymbol{r})\phi_k(\boldsymbol{r}), \tag{2}$$

and the corresponding odd electron number is given by

$$n_k^{\mathrm{odd}} = \mathrm{Tr}D_k^{\mathrm{odd}}(\boldsymbol{r}) = \min(2 - n_k, n_k). \tag{3}$$

Thus, for $n_k \leq 1$, n_k^{odd} corresponds to the occupation number while for $n_k \geq 1$, $n_k^{\mathrm{odd}} = 2 - n_k$ is the complement to achieve a closed shell. In other words, the $\min(2 - n_k, n_k)$ factor can be regarded as the probability for the electron of being unpaired in $\phi_k(\boldsymbol{r})$. The total odd electron number is then given by

$$N^{\mathrm{odd}} = \sum_{k=1}^{M} n_k^{\mathrm{odd}} \quad (N^{\mathrm{odd}} \leq N), \tag{4}$$

where N is the total number of electrons. Now, let us consider for the sake of simplicity a singlet system with an even number of electrons ($N_\alpha = N_\beta$); the extension to the case of $N_\alpha \neq N_\beta$ is however straightforward [57]. In that case, the use of Eq. 3 is consistent with the conventional measure of the diradical character y_i ($0 \leq y_i \leq 1$) defined from the occupation number of the LUNO + i ($i = 0$, 1,…), i.e., $n_{\mathrm{LUNO}+i}$. Since the $n_{\mathrm{HONO}-i} + n_{\mathrm{LUNO}+i} = 2$ condition is satisfied for the spin-unrestricted Hartree–Fock (UHF) and DFT (UDFT) methods,

$$D_{\mathrm{HONO}-i}(\boldsymbol{r}) = D_{\mathrm{LUNO}+i}(\boldsymbol{r}), \tag{5}$$

which is only approximately satisfied in general multi-determinant methods, and we can rewrite the diradical character as

$$\begin{aligned} y_i &\equiv \frac{1}{2}\mathrm{Tr}[D_{\mathrm{HONO}-i}(\boldsymbol{r}) + D_{\mathrm{LUNO}+i}(\boldsymbol{r})] = \frac{1}{2}\mathrm{Tr}\left[D_{y_i}^{\mathrm{odd}}(\boldsymbol{r})\right] \\ &= \frac{1}{2}\left(n_{\mathrm{HONO}-i}^{\mathrm{odd}} + n_{\mathrm{LUNO}+i}^{\mathrm{odd}}\right) = \frac{1}{2}n_{y_i}^{\mathrm{odd}}, \end{aligned} \tag{6}$$

where $y_i = n_{\mathrm{HONO}-i}^{\mathrm{odd}} = n_{\mathrm{LUNO}+i}^{\mathrm{odd}}$ is satisfied and the odd electron number and density for y_i are defined as $n_{y_i}^{\mathrm{odd}} \equiv 2y_i$. and $D^{y_i}(\boldsymbol{r})$, respectively. Therefore, from Eqs. 2 to 6, the total odd electron density within single-determinant schemes is expressed in two different but equivalent ways:

$$D(\boldsymbol{r}) = \sum_{k=1}^{M} D_k(\boldsymbol{r}) = \sum_{i=0}^{N/2-1} D^{y_i}(\boldsymbol{r}), \tag{7}$$

which describe the spatial distribution of all the odd electrons. Note that the first equality in Eq. 7, which is also valid for any multi-determinant method, provides an alternative exact partitioning scheme of the odd electron density into each NO contribution. It can be noted that the factor in front of the $\phi_k^*(\boldsymbol{r})\phi_k(\boldsymbol{r})$ term in Eq. 2 represents the intensity factor contributing to the density $D_k^{\mathrm{odd}}(\boldsymbol{r})$, and there is an infinite number of ways of defining such factors that satisfy the intuitively obvious limits ($n_k = 0$, 1, and 2). We have chosen the one due to Head-Gordon (Eq. 2) [57] because it does not exaggerate the diradical character and the total odd electron number, particularly in the intermediate diradical character region, in contrast to Takatsuka's definition, $n_k(2 - n_k)$, which does [55].

On the other hand, the chemical and physical properties like the optical and magnetic responses should be calculated using the one-electron reduced density (not odd electron density), which for any single-determinant method is given by

$$\begin{aligned} d(\boldsymbol{r}) &= \sum_{i=0}^{N/2-1} \left[n_{\mathrm{HONO}-i}\phi_{\mathrm{HONO}-i}^*(\boldsymbol{r})\phi_{\mathrm{HONO}-i}(\boldsymbol{r}) \right. \\ &\quad \left. + n_{\mathrm{LUNO}+i}\phi_{\mathrm{LUNO}+i}^*(\boldsymbol{r})\phi_{\mathrm{LUNO}+i}(\boldsymbol{r})\right] \\ &\equiv \sum_{i=0}^{N/2-1} d^{y_i}(\boldsymbol{r}), \end{aligned} \tag{8}$$

where $d^{y_i}(\boldsymbol{r})$ indicates the one-electron reduced density corresponding to y_i.

2.2 Partitioning of the (hyper)polarizability density into natural orbitals and/or diradical characters contributions

Under the influence of a static electric field $\boldsymbol{F}$, the electronic Hamiltonian H for a N-electron system (in a.u.) is given by

$$H = -\frac{1}{2}\sum_{i=1}^{N}\nabla_i^2 - \sum_{i=1}^{N}\sum_{X}\frac{Z_X}{r_{iX}} + \sum_{i=1}^{N}\sum_{j>i}^{N}\frac{1}{r_{ij}} + \sum_{i=1}^{N}\boldsymbol{F}\cdot\boldsymbol{r}_i. \tag{9}$$

In this case, the molecule exhibits an electric polarization $\boldsymbol{p}$ or dipole moment. We consider a simple definition of the (hyper)polarizability and of its density [52] based on Eq. 8, which can lead to the partitioning of the total (hyper)polarizability and of its density into those corresponding to each diradical character. Such a partitioning is only meaningful provided $n_{\mathrm{HONO}-i} + n_{\mathrm{LUNO}+i} = 2$ (See Sect. 2.1). The (hyper)polarizabilities are defined by the expansion coefficients of the polarization p^a as a function of the applied electric field F:

$$\begin{aligned} p^a &\equiv -\int r_a d(\boldsymbol{r})d\boldsymbol{r} \\ &= \mu_0^a + \sum_b \alpha_{ab}F^b + \sum_{b,c}\beta_{abc}F^bF^c + \sum_{b,c,d}\gamma_{abcd}F^bF^cF^d \\ &\quad + \cdots, \end{aligned} \tag{10}$$

where the one-electron reduced density $d(\boldsymbol{r})$ is also expanded as

$$\begin{aligned} d(\boldsymbol{r}) &= d^{(0)}(\boldsymbol{r}) + \sum_b d_b^{(1)}(\boldsymbol{r})F^b + \frac{1}{2!}\sum_{b,c} d_{bc}^{(2)}(\boldsymbol{r})F^bF^c \\ &\quad + \frac{1}{3!}\sum_{b,c,d} d_{bcd}^{(3)}(\boldsymbol{r})F^bF^cF^d + \cdots. \end{aligned} \tag{11}$$

By combining these equations, in the static case, the polarizability (α_{ab}), the first (β_{abc}) and the second

(γ_{abcd}) hyperpolarizabilities (a, b, c, $d = x$, y, z) are given by

$$\alpha_{ab} = -\int r_a d_b^{(1)}(\boldsymbol{r})d\boldsymbol{r} = \sum_{i=0}^{N/2-1}\left(-\int r_a d_b^{y_i(1)}(\boldsymbol{r})d\boldsymbol{r}\right) \equiv \sum_{i=0}^{N/2-1}\alpha_{ab}^{y_i}, \tag{12}$$

$$\beta_{abc} = -\frac{1}{2!}\int r_a d_{bc}^{(2)}(\boldsymbol{r})d\boldsymbol{r} = \sum_{i=0}^{N/2-1}\left(-\frac{1}{2!}\int r_a d_{bc}^{y_i(2)}(\boldsymbol{r})d\boldsymbol{r}\right) \equiv \sum_{i=0}^{N/2-1}\beta_{abc}^{y_i}, \tag{13}$$

and

$$\gamma_{abcd} = -\frac{1}{3!}\int r_a d_{bcd}^{(3)}(\boldsymbol{r})d\boldsymbol{r} = \sum_{i=0}^{N/2-1}\left(-\frac{1}{3!}\int r_a d_{bcd}^{y_i(3)}(\boldsymbol{r})d\boldsymbol{r}\right) \equiv \sum_{i=0}^{N/2-1}\gamma_{abcd}^{y_i}. \tag{14}$$

Here, $\alpha_{ab}^{y_i}$, $\beta_{abc}^{y_i}$ and $\gamma_{abcd}^{y_i}$ are the electron (hyper) polarizabilities corresponding to y_i, and their densities are given by

$$d_b^{y_i(1)}(\boldsymbol{r}) = \left.\frac{\partial d^{y_i}(\boldsymbol{r})}{\partial F_b}\right|_{\boldsymbol{F}=0}, \tag{15}$$

$$d_{bc}^{y_i(2)}(\boldsymbol{r}) = \left.\frac{\partial^2 d^{y_i}(\boldsymbol{r})}{\partial F_b \partial F_c}\right|_{\boldsymbol{F}=0}, \tag{16}$$

and

$$d_{bcd}^{y_i(3)}(\boldsymbol{r}) = \left.\frac{\partial^3 d^{y_i}(\boldsymbol{r})}{\partial F_b \partial F_c \partial F_d}\right|_{\boldsymbol{F}=0}, \tag{17}$$

and the total (hyper)polarizability densities are expressed by

$$d_b^{(1)}(\boldsymbol{r}) = \sum_{i=0}^{N/2-1} d_b^{y_i(1)}(\boldsymbol{r}), \tag{18}$$

$$d_{bc}^{(2)}(\boldsymbol{r}) = \sum_{i=0}^{N/2-1} d_{bc}^{y_i(2)}(\boldsymbol{r}), \tag{19}$$

and

$$d_{bcd}^{(3)}(\boldsymbol{r}) = \sum_{i=0}^{N/2-1} d_{bcd}^{y_i(3)}(\boldsymbol{r}). \tag{20}$$

In our investigations, the derivatives of the electron density with respect to the electric field (see Eqs. 12–17) are referred to as the (hyper)polarizability densities, while in the terminology used by Hunt [66–68], the whole integrands are called $(n-1)$th reduced densities, e.g., the reduced polarizability density in the case of α_{ab}, the doubly reduced density in the case of β_{abc}, and so on.

The contributions obtained from a pair of positive and negative (hyper)polarizability densities provide a description of the local electronic contributions to the total (hyper)polarizability. The positive and negative values of the (hyper)polarizability densities represent, respectively, the successive orders of the field-induced increases and decreases in the charge density, which determine the nth-order dipole moment in the direction from positive to negative (hyper)polarizability densities. So, any (hyper) polarizability density map represents the relative phase and magnitude of the change in the nth-order densities between two spatial points with positive and negative values. In other words, the (hyper)polarizability density analysis provides a chemical local view of the molecular (non)linear optical responses: it is useful not only for assessing the reliability of methods and basis sets employed, but also for illuminating the primary contributions of electrons, orbitals, substituents, π-conjugated linkers to the (hyper) polarizabilities [69–71]. An advantage of the partitioning into the diradical character contribution is to highlight the contribution of each diradical pair (or each NO pair) in a multi-radical system. Actually, the partitioning into contributions from NOs satisfying $0 < y_i \leq 1$ and the rest giving $y_i \sim 0$ is further useful for clarifying the effects originating from the open-shell character because the (hyper)polarizabilities enhancement in open-shell molecules is predicted to be mainly caused by the odd electrons with intermediate y_i values [42–44].

2.3 Approximate spin projection scheme for the (hyper)polarizabilities and their densities within spin-unrestricted single-determinant methods

Spin-unrestricted single-determinant methods are known to suffer from spin contamination, which leads, e.g., to small humps in the potential energy curve in the intermediate bond dissociation region [58], to wrong optimized structures of open-shell molecules [59], and to incorrect diradical character dependences of the (hyper)polarizabilities of open-shell singlet molecules [42]. Although several effective approaches to remove spin contamination have been proposed, e.g., the spin-flip methods due to Krylov [72, 73] and the approximate spin projection methods based on the Heisenberg model by Yamaguchi [58], they still present difficulties to be applied to delocalized multi-radical π-conjugated systems. Here, we present an alternative approximate method for removing spin contamination effects on the (hyper)polarizability by resorting to the perfect-pairing spin projection scheme [41, 55, 60] applied to the occupation numbers n_k^{U} obtained using spin-unrestricted single-determinant methods (in Sect. 2.1 we omitted for simplicity the U superscript):

$$n^{\mathrm{SP}}_{\mathrm{HONO}-i} = \frac{\left(n^{\mathrm{U}}_{\mathrm{HONO}-i}\right)^2}{1+\left(S^{\mathrm{U}}_i\right)^2} \equiv 2 - y^{\mathrm{SP}}_i, \text{ and}$$
$$n^{\mathrm{SP}}_{\mathrm{LUNO}+i} = \frac{\left(n^{\mathrm{U}}_{\mathrm{LUNO}+i}\right)^2}{1+\left(S^{\mathrm{U}}_i\right)^2} \equiv y^{\mathrm{SP}}_i, \quad (21)$$

where S^{U}_i, the overlap between the corresponding orbital pairs, is given by

$$S^{\mathrm{U}}_i = \frac{n^{\mathrm{U}}_{\mathrm{HONO}-i} - n^{\mathrm{U}}_{\mathrm{LUNO}+i}}{2}. \quad (22)$$

y^{SP}_i corresponds to the spin projected diradical character defined by Yamaguchi [34], which coincides with Eq. 6, provided n^{SP}_k is used in Eq. 3. By using these spin projected occupation numbers in Eqs. 2–4, 6, and 8, we can define approximate spin projected odd electron density $\left[D^{\mathrm{SP}}_k(\boldsymbol{r}), D^{y_i\ \mathrm{SP}}(\boldsymbol{r})\right]$, total odd electron number ($N^{\mathrm{odd\,SP}}$), and one-electron reduced density $[d^{y_i\ \mathrm{SP}}(\boldsymbol{r}), d^{\mathrm{SP}}(\boldsymbol{r})]$. Here, "approximate" means that the spin projection is performed only on the occupation numbers, not on the NOs. For instance, the spin projected one-electron density $d^{\mathrm{SP}}(\boldsymbol{r})$ is expressed by

$$d(\boldsymbol{r}) = \sum_{i=0}^{N/2-1} \left[n^{\mathrm{SP}}_{\mathrm{HONO}-i}\phi^*_{\mathrm{HONO}-i}(\boldsymbol{r})\phi_{\mathrm{HONO}-i}(\boldsymbol{r}) + n^{\mathrm{SP}}_{\mathrm{LUNO}+i}\phi^*_{\mathrm{LUNO}+i}(\boldsymbol{r})\phi_{\mathrm{LUNO}+i}(\boldsymbol{r})\right] \equiv \sum_{i=0}^{N/2-1} d^{y_i\ \mathrm{SP}}(\boldsymbol{r}). \quad (23)$$

Similarly, we can define spin projected (hyper) polarizabilities $\left(\alpha^{\mathrm{SP}}_{ab}, \beta^{\mathrm{SP}}_{abc}, \gamma^{\mathrm{SP}}_{abcd}\right)$ and their densities $\left(d^{(1)\ \mathrm{SP}}_a, d^{(2)\ \mathrm{SP}}_{ab}, d^{(3)\ \mathrm{SP}}_{abc}\right)$ by using the spin projected one-electron reduced densities in Eqs. 12–20. In practice, to calculate the spin projected charge density and the (hyper)polarizabilities, we only need to replace the one-electron reduced charge densities $d^{y_i}(\boldsymbol{r})$ by $d^{y_i\ \mathrm{SP}}(\boldsymbol{r})$ in case of $y_i \neq 0$ or 1, because the occupation numbers for $n^{\mathrm{odd}}_k = 0, 1$ and 2 do not change by this spin projection (see Eqs. 21 and 22). As a consequence, since the weights of the different NOs are modified upon spin projection, the whole one-electron reduced density and the (hyper)polarizability densities can change not only quantitatively, but also qualitatively.

3 Illustrative applications on 1,3-dipoles and rectangular graphene nanoflakes

In order to illustrate the present method, we examined typical open-shell singlet systems, i.e., 1,3-dipole (Fig. 1) and rectangular graphene nanoflakes PAH[*X*,*Y*] (Fig. 2) [20], where *X* and *Y* denote the number of fused rings in the zigzag and armchair edges, respectively. The 6-31G** + *pd* basis sets ($\zeta_{p,d} = 0.0523$ on C atom, 0.0582 on N atom, and 0.0719 on O atom) were employed for the calculations on the 1,3-dipole systems. Though for small compounds, the use of the extended basis sets including polarization and diffuse functions is necessary for obtaining quantitative γ values of [74], this is not the case for extended π-conjugated systems. So, the standard 6-31G* basis set was chosen for PAH systems. This choice has been substantiated in our previous study where the 6-31G* basis set underestimates the γ value of *s*-indaceno[1,2,3-*cd*;5,6,7-*c*′*d*′]diphenalene (IDPL), which is a singlet polycyclic aromatic diradical system involving two phenalenyl radical rings, by only 10% with respect to the 6-31G* + diffuse *p* ($\zeta = 0.0523$) basis set [45, 46]. Other related computational issues are discussed in Refs. [75, 76].

The LC-UBLYP/6-31G* method is adopted to calculate γ because it alleviates its catastrophic DFT overestimation, which has been observed for extended π-conjugated systems when using conventional exchange–correlation functionals [77–84], and because it closely reproduces the reference UCCSD(T) γ values of open-shell singlet

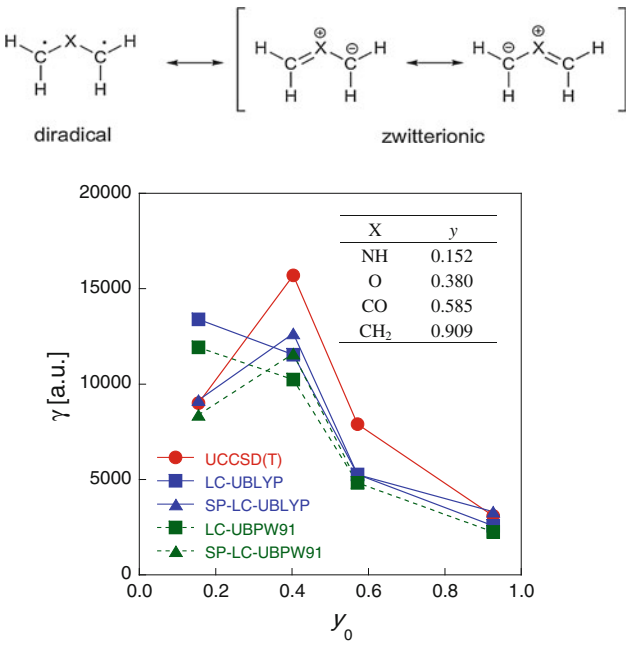

Fig. 1 Resonance structures and second hyperpolarizabilities in 1,3-dipole systems $(CH_2)X(CH_2)$. The γ values are presented as a function of the diradical character y_0, which is influenced by the nature of the X group (=NH, O, CO, CH_2). The diagonal component of the γ tensor along the CC axis is calculated at the UCCSD(T), LC-UBLYP ($\mu = 0.47$), SP-LC-UBLYP($\mu = 0.47$), LC-UBPW91($\mu = 0.47$), and SP-LC-UBPW91($\mu = 0.47$) levels using the 6-31G** + *sp* basis sets, and y_0 value is obtained from UHF NO occupation numbers

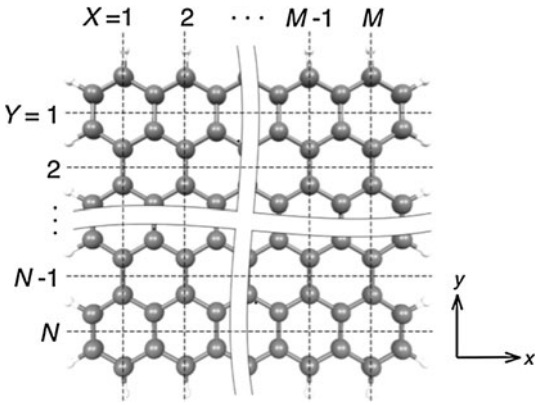

Fig. 2 Rectangular graphene nanoflake PAH[*X*,*Y*], where *X* and *Y* denote the number of fused rings in the zigzag and armchair edges, respectively. Carbon (C) and hydrogen (H) atoms are shown in black and white, respectively, as well as coordinate axes

molecules with intermediate and large diradical characters, provided that the range separating parameter μ amounts to 0.3–0.5 [61, 85]. Moreover, for model open-shell singlet molecules, the UCCSD(T) method reproduces well Full CI γ values [86]. In this study, we employed the standard $\mu = 0.47$ value, which has been optimized to minimize the errors in the atomization energies of molecules in the G2 set [87] and which is implemented in the Gaussian 09 program [88]. For several PAHs[*X*,*Y*], the odd electron densities are localized on the zigzag edges, so that the spin-polarization direction is parallel to the armchair edge (*y*-axis). Therefore, the intermediate diradical character originating from the odd electron densities on these zigzag edges (see Figs. 3 and 6) is responsible for the enhancement of γ_{yyyy} (parallel to the armchair edge) when compared with γ_{xxxx} (parallel to the zigzag edge) [49]. The geometries have been optimized at the UB3LYP/6-31G* level.

A recent work due to Filatov and Cramer suggested that specific response properties should be calculated with the PW91 rather than with the LYP correlation functional because LYP exaggerates opposite-spin correlation effects and invokes an exaggerated spin-polarization pattern in the core shells of the atoms [89]. However, since the (hyper)polarizability of open-shell systems with intermediate diradical characters originates primarily from the valence-shell unpaired electrons, these properties are not expected to change upon switching to the LC-UBPW91 method. This was confirmed by considering the 1,3-dipoles (as shown in the next section, Fig. 1): the LC-UBPW91 and LC-UBLYP γ values are similar as well as for their spin projected counterparts. Nevertheless, the PW91 γ amplitudes are slightly smaller than those obtained using the LYP functional.

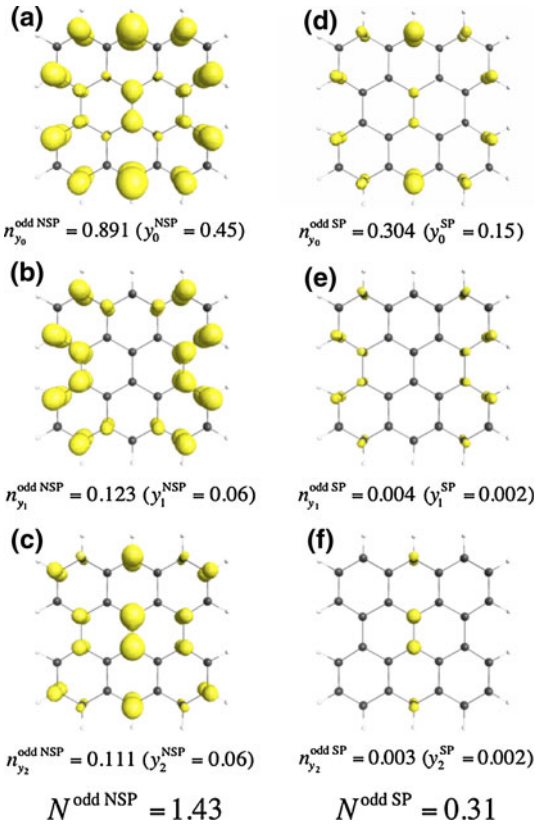

Fig. 3 Non-spin projected and spin projected odd electron densities [$D^{y_i\ \text{NSP}}(\boldsymbol{r})$, $D^{y_i\ \text{SP}}(\boldsymbol{r})$] as well as odd electron numbers ($n_{y_i}^{\text{odd NSP}}$, $n_{y_i}^{\text{odd SP}}$) corresponding to the diradical characters y_0^{NSP} (**a**), y_1^{NSP} (**b**), y_2^{NSP} (**c**), y_0^{SP} (**d**), y_1^{SP} (**e**) and y_2^{SP} (**f**) of PAH[3,3] calculated by the LC-UBLYP/6-31G* method. The yellow surfaces represent densities with iso-surfaces of 0.0015 a.u. ($i = 0$) and 0.0003 a.u. ($i = 1, 2$)

3.1 1,3-Dipole systems: comparison between SP-LC-UBLYP and UCCSD(T)

To assess the performance of the spin projected (SP)-LC-UBLYP method, we considered typical diradical systems, 1,3-dipoles, $(CH_2)X(CH_2)$ (X = NH, O, CO, CH_2), which span a wide range of diradical character by changing the central atom [61]. The γ tensor component along the CC axis was calculated with this method and compared with non-spin projected (NSP)-LC-UBLYP and UCCSD(T) results. The y_0 values were calculated from the SP form (Eqs. 21 and 22) using the UHF NOs (HONO and LUNO). As shown in Fig. 1, the SP scheme improves the γ values in the relatively small y_0 region where it corrects the overshot LC-UBLYP γ and, therefore, the description of the dependence of γ over the whole diradical character range, for instance, when X = NH, $\gamma = 9.0 \times 10^3$ a.u. (100%) [UCCSD(T)], 13.4×10^3 a.u. (149%) (LC-UBLYP) and 9.2×10^3 a.u. (102%) (SP-LC-UBLYP). Nevertheless, the SP-LC-UBLYP method still undershoots the UCCSD(T) γ

value in the intermediate y_0 value region: for X = O, $\gamma = 15.7 \times 10^3$ a.u. (100%) [UCCSD(T)], 11.5×10^3 a.u. (73%) (LC-UBLYP), and 12.7×10^3 a.u. (81%) (SP-LC-UBLYP). From these results, the SP-LC-UBLYP scheme is expected to provide semi-quantitative diradical character dependences of γ for π-conjugated diradical molecules.

3.2 PAH[3,3], a diradical system

Owing to its intermediate y_0 value and its much smaller y_i ($i \geq 1$) values (calculated from the spin projected UHF NO occupation numbers [41]), PAH[3,3] has been described as a diradical molecule with an intermediate diradical character [20]. In order to investigate the partitioning of the total γ_{yyyy} value and of its density into those corresponding to the successive y_i ($i \geq 0$), y_i was calculated from the NO occupation numbers calculated by the LC-UBLYP/6-31G* method, which conserves the qualitative picture obtained at the UHF level. Indeed, at the LC-UBLYP/6-31G* level, $y_0^{\mathrm{NSP}} = 0.45$ while $y_i^{\mathrm{NSP}} < 0.1$ ($i \geq 1$) (see Table 1). Note that we examine first the non-spin projected (NSP) results, i.e., the spin-unrestricted (U) DFT ones, and then we will focus on the SP results. Table 1 also lists the total and partitioned γ_{yyyy} values $\left[\gamma_{yyyy}^{y_0}, \gamma_{yyyy}^{\mathrm{rest}} (\equiv \gamma_{yyyy} - \gamma_{yyyy}^{y_0})\right]$ of PAH[3,3]. Nevertheless, before discussing the partitioned values, we look at the difference in γ_{yyyy} amplitudes between the present and previous results, i.e., 91.4×10^3 a.u. (LC-UBLYP/6-31G*) and 145×10^3 a.u. (UBHandHLYP/6-31G*) [16]. Judging from the good agreement between UBHandHLYP and LC-UBLYP γ_{yyyy} values for relatively small-size open-shell singlet systems [61, 85], the UBHandHLYP γ_{yyyy} value for PAH[3] is presumed to suffer from the catastrophic DFT overestimation of γ in extended conjugated systems [77–84]. This also rationalizes the use of the LC-UBLYP method for PAH[*X*,*Y*]s with different *X* and *Y* values.

For $\gamma_{yyyy}^{y_0\ \mathrm{NSP}}$, we obtain a value of 39.3×10^3 a.u., which attains 43% of the total γ_{yyyy}. The associated odd electron density $[D^{y_0\ \mathrm{NSP}}(\boldsymbol{r})]$ shown in Fig. 3a displays the largest amplitudes in the middle region on both the zigzag edges and the armchair atoms next to the zigzag edges. Upon integration, one obtains a value of 0.89 for $n_{y_0}^{\mathrm{odd\,NSP}} \left(\equiv n_{\mathrm{HONO}}^{\mathrm{odd\,NSP}} + n_{\mathrm{LUNO}}^{\mathrm{odd\,NSP}}\right)$, which corresponds to the dominant contribution (62%) to the total odd electron number, $N^{\mathrm{odd\,NSP}}$, amounting to 1.43. Two additional odd electron numbers of 0.23 (16%) originate from y_1 and y_2 while their odd electron densities are covering similar as well as complementary C sites of PAH[3] (Fig. 3b and c). Figure 4a and b shows the $\gamma_{yyyy}^{\mathrm{NSP}}$ and $\gamma_{yyyy}^{y_0\ \mathrm{NSP}}$ density distributions, respectively. The density distribution pattern of $\gamma_{yyyy}^{\mathrm{NSP}}$ displays similarities with that of $\gamma_{yyyy}^{y_0\ \mathrm{NSP}}$, though the $\gamma_{yyyy}^{y_0\ \mathrm{NSP}}$ density amplitudes are smaller on the zigzag edges and larger in the internal region than the $\gamma_{yyyy}^{\mathrm{NSP}}$ density amplitudes. Moreover, the $\gamma_{yyyy}^{\mathrm{NSP}}$ density pattern reflects that of odd electron density $D^{y_0\ \mathrm{NSP}}(\boldsymbol{r})$ (see Figs. 3a and 4a) and, to a minor extent, $D^{y_1\ \mathrm{NSP}}(\boldsymbol{r})$ and $D^{y_2\ \mathrm{NSP}}(\boldsymbol{r})$ (see Fig. 3b and c). These results exemplify that the $\gamma_{yyyy}^{\mathrm{NSP}}$ of PAH[3,3] is mostly characterized by the contribution of odd electrons with intermediate $y_0^{\mathrm{NSP}} (= 0.45)$, though remaining contributions are correlated with y_i ($i \geq 1$). It is also important to emphasize on the point that the partitioning of the hyperpolarizabilities into NOs contributions is a subtle issue.

Table 1 Non-spin projected (NSP) and spin projected (SP) diradical characters (y_0) and second hyperpolarizabilities $\left[\gamma_{yyyy}^{y_0}, \gamma_{yyyy}^{\mathrm{rest}} (\equiv \gamma_{yyyy} - \gamma_{yyyy}^{y_0})\right]$ ($\times 10^3$ a.u.) of PAH[3,3] calculated by the LC-UBLYP/6-31G* method

	NSP	SP
y_0	0.45	0.15
$\gamma_{yyyy}^{y_0}$	39.3 (43%)	56.1 (55%)
$\gamma_{yyyy}^{\mathrm{rest}}$	52.1 (57%)	45.0 (45%)
γ_{yyyy}	91.4	101.1

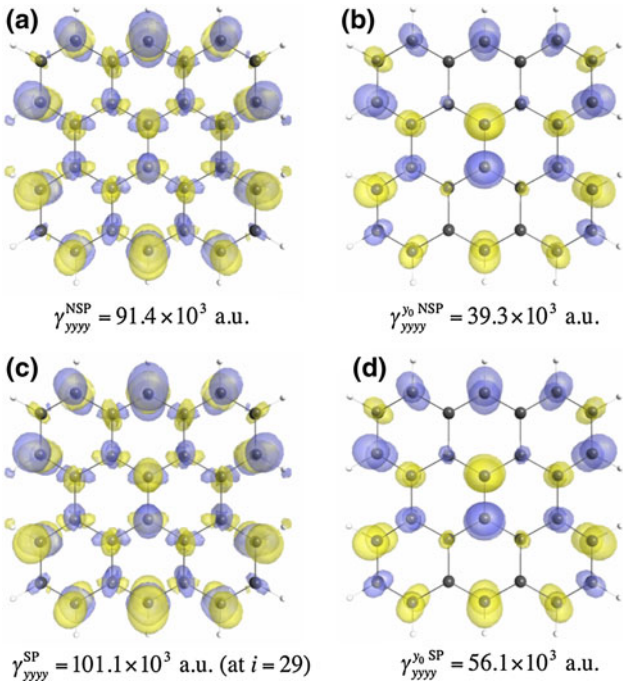

Fig. 4 Non-spin projected and spin projected γ_{yyyy} [$\gamma_{yyyy}^{\mathrm{NSP}}$ (**a**), $\gamma_{yyyy}^{y_0\ \mathrm{NSP}}$ (**b**), $\gamma_{yyyy}^{\mathrm{SP}}$ (**c**), $\gamma_{yyyy}^{y_0\ \mathrm{SP}}$ (**d**)] density distributions of PAH[3,3] calculated by the LC-UBLYP/6-31G* method. The yellow and blue meshes represent positive and negative densities with iso-surface ±300 a.u., respectively

Indeed, going from the highest occupied level to lower ones, the individual contributions increase in amplitude, but their signs alternate so that they mostly cancel. The analysis should therefore concentrate on the response of the highest levels, which, as shown here for the HONO and LUNO, exhibit the same third-order field-induced pattern as the full response.

Next, we examine the spin projection effects (see "NSP" and "SP" values in Table 1) by employing Eqs. 21 and 22 on the occupation numbers of the HONO $- i$ and LUNO $+ i$ with i ranging from 0 to 29. The spin projected γ_{yyyy} values nicely converge with $i_{\max}$ (the largest NO number included in the SP scheme) and saturate around $i_{\max} = 13$ as shown in Fig. 5a. The enhancement ratio with respect to the non-spin projected γ_{yyyy} value $\left[= \left(\gamma_{yyyy}^{\mathrm{SP}}/\gamma_{yyyy}^{\mathrm{NSP}} - 1\right) \times 100\right]$ is the largest at $i_{\max} = 0$ (18% at $i_{\max} = 0$ vs. 11% at $i_{\max} = 29$). Concomitantly, the y_0 value is reduced by 67% (0.45 → 0.15) by the spin projection. Accordingly, the amplitude of the odd electron density distribution of $D^{y_0\,\mathrm{SP}}(\boldsymbol{r})$ $\left[n_{y_0}^{\mathrm{odd\,SP}}(\equiv n_{\mathrm{HONO}-1}^{\mathrm{odd\,SP}} + n_{\mathrm{LUNO}+1}^{\mathrm{odd\,SP}}) = 0.30\right]$ is strongly reduced (see Fig. 3d). The same occurs for the next NO pairs (see Fig. 3e and f). Then, the total odd electron number $N^{\mathrm{odd\,SP}}$ is also reduced to 0.31 (with respect to $N^{\mathrm{odd\,NSP}} = 1.43$), which indicates that PAH[3] should be regarded as an open-shell singlet system with a small diradical character. Such reductions in the diradical character and the odd electron density are caused by removing the spin contaminations. In contrast, the spin projection effect only increases γ_{yyyy} [$\gamma_{yyyy}^{\mathrm{SP}} = 101.1 \times 10^3$ a.u. (at $i_{\max} = 29$)] by 11% relative to $\gamma_{yyyy}^{\mathrm{NSP}}$ [91.4×10^3 a.u.] (see Table 1). This increase is principally caused by the significant increase [$\sim$43% or (16.8×10^3 a.u.)] in $\gamma_{yyyy}^{y_0\,\mathrm{SP}}$ relative to $\gamma_{yyyy}^{y_0\,\mathrm{NSP}}$ and the decrease in the remaining contributions ($\gamma_{yyyy}^{\mathrm{rest}}$) [$\sim$14% ($7.1 \times 10^3$ a.u.)]. As a result, the contribution of $\gamma_{yyyy}^{y_0}$ to the total γ_{yyyy} increases from 43 to 55%, while the remaining contribution decreases from 57 to 45%. Figure 4c and d shows the $\gamma_{yyyy}^{\mathrm{SP}}$ and $\gamma_{yyyy}^{y_0\,\mathrm{SP}}$ density distributions, respectively, in which the $\gamma_{yyyy}^{\mathrm{SP}}$ density distribution well reflects the $\gamma_{yyyy}^{y_0\,\mathrm{SP}}$ density distribution. Both the amplitude and the distribution pattern of the $\gamma_{yyyy}^{\mathrm{SP}}$ $\left(\gamma_{yyyy}^{y_0\,\mathrm{SP}}\right)$ density are similar to those of $\gamma_{yyyy}^{\mathrm{NSP}}$ $\left(\gamma_{yyyy}^{y_0\,\mathrm{NSP}}\right)$ density, as expected from the relatively small differences between the $\gamma_{yyyy}^{\mathrm{SP}}\left(\gamma_{yyyy}^{y_0\,\mathrm{SP}}\right)$ and $\gamma_{yyyy}^{\mathrm{NSP}}$ $\left(\gamma_{yyyy}^{y_0\,\mathrm{NSP}}\right)$ values. Finally, like for the NSP case, the $\gamma_{yyyy}^{y_0\,\mathrm{SP}}$ density reflects $D^{y_0\,\mathrm{SP}}(\boldsymbol{r})$ (see Fig. 3d) and, to a lower though visible extent, $D^{y_1\,\mathrm{SP}}(\boldsymbol{r})$ and $D^{y_2\,\mathrm{SP}}(\boldsymbol{r})$ (see Fig. 3e and f).

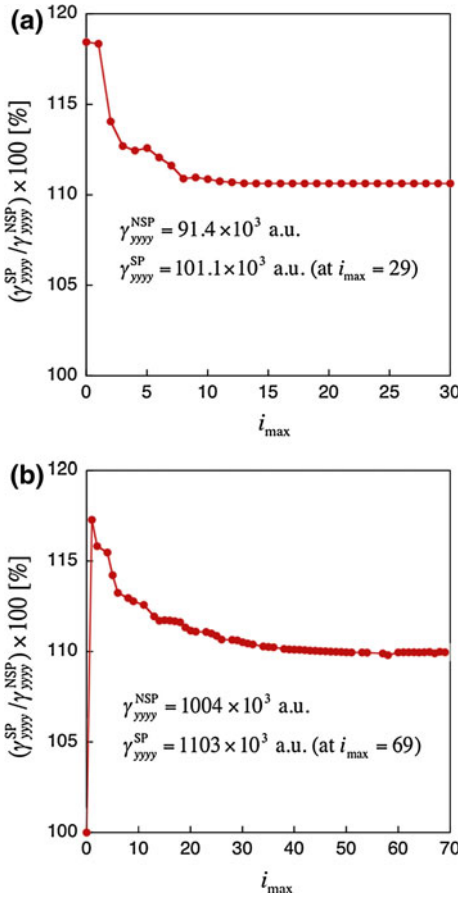

Fig. 5 $\gamma_{yyyy}^{\mathrm{SP}}/\gamma_{yyyy}^{\mathrm{NSP}}$ ratio as a function of $i_{\max}$, the largest NO number (HONO-i and LUNO + i, $i = 0,\ldots, i_{\max}$) included in the SP scheme, for PAH[3,3] (**a**) and PAH[6,7] (**b**) calculated by the LC-UBLYP/6-31G* method

3.3 PAH[6,7], a multi-radical system

In contrast to PAH[3,3], PAH[6,7] displays an intermediate y_1 value, while $y_0 \sim 1$ and $y_i \sim 0$ ($i \geq 2$) (calculated from the spin projected UHF NO occupation numbers). This suggests that PAH[6,7] (see Fig. 2) has a tetra-radical character [20]. Indeed, γ_{yyyy} of PAH[X,7] shows a unique increasing behavior with X: the maxima of γ_{yyyy} appear at $X = 2$ and 6. This was explained to be a signature of the (intermediate) tetra-radical character of PAH[6,7] and of the (intermediate) diradical character of PAH[2,7]: the enhancement of γ_{yyyy} of PAH[2,7] is dominantly caused by the intermediate y_0, while that of PAH[6,7] is done by the intermediate y_1 [20]. In order to clarify this multi-radical effect, we partition the total γ_{yyyy} values into those corresponding to the principal y_i ($i = 0$, 1) and the rest. The diradical characters evaluated from the NO occupation numbers calculated by the LC-UBLYP/6-31G* method point out the pure diradical character of the (HONO,

LUNO) pair $\left(y_0^{\mathrm{NSP}} \sim 1\right)$ and a relatively large diradical character for the (HONO-1, LUNO + 1) pair $\left(y_1^{\mathrm{NSP}} = 0.75\right)$ (Table 2). Concerning the non-spin projected (NSP) γ results, the difference in γ_{yyyy} amplitudes between the present [1,004 × 10^3 a.u. (LC-UBLYP/6-31G*)] and the previous [2,150 × 10^3 a.u. (UBHandHLYP/6-31G*) [20]] is substantial and is larger in PAH[6,7] than in PAH[3], as it could have been expected since the system is larger. This also indicates that the use of LC-UBLYP method is preferable for determining the γ values of PAH[6,7]. The relative contribution to $\gamma_{yyyy}^{\mathrm{NSP}}$ from the NOs with $y_0^{\mathrm{NSP}} \sim 1$ is negligible $\left(\gamma_{yyyy}^{y_0\,\mathrm{NSP}} = -3 \times 10^3 \text{ a.u.}\right)$ while that with $y_1^{\mathrm{NSP}} = 0.75$ attains 153 × 10^3 a.u. (15%), which is significantly smaller than the contribution from all the remaining electrons [854 × 10^3 a.u. (85%)]. This suggests that the remaining orbitals ($i \geq 2$) still include many open-shell orbitals with smaller diradical characters. Indeed, the odd electron densities [$D^{y_i\,\mathrm{NSP}}(\boldsymbol{r})$, $i = 0, 1$] shown in Fig. 6a and b integrate to an odd electron number of 3.49, in comparison with the total $N^{\mathrm{odd\,NSP}}$ value of 6.26, substantiating the fact there remains a comparable number of odd electrons in the NOs with $i \geq 2$. $D^{y_0\,\mathrm{NSP}}(\boldsymbol{r})$ $\left[n_{y_0}^{\mathrm{odd\,NSP}}(\equiv n_{\mathrm{HONO}}^{\mathrm{odd\,NSP}} + n_{\mathrm{LUNO}}^{\mathrm{odd\,NSP}}) = 2.00\right]$ presents significant amplitudes on both zigzag edges (in particular in the middle region) while $D^{y_1\,\mathrm{NSP}}(\boldsymbol{r})$ $\left[n_{y_1}^{\mathrm{odd\,NSP}}\left(\equiv n_{\mathrm{HONO-1}}^{\mathrm{odd\,NSP}} + n_{\mathrm{LUNO+1}}^{\mathrm{odd\,NSP}}\right) = 1.49\right]$ is also distributed on the zigzag edges, though not in the middle, and inside the zigzag edges. Thus, the diradical pairs contributing to the multi-radical character present clearly distinct odd electron density distributions. The relative density distribution of $\gamma_{yyyy}^{y_0\,\mathrm{NSP}}$ is negligible and not represented. On the other hand, there are similarities between the density distribution patterns of $\gamma_{yyyy}^{\mathrm{NSP}}$ and $\gamma_{yyyy}^{y_1\,\mathrm{NSP}}$ (Fig. 7a and b), but obviously, their amplitudes are different, in particularly in the four-corner phenalenyl blocks. These results demonstrate that the relationship between the diradical character and γ obtained for diradical molecules can be generalized to multi-radical systems with non-zero y_i ($i \geq 1$).

Table 2 Non-spin projected (NSP) and spin projected (SP) diradical characters (y_0,y_1) and second hyperpolarizabilities [$\gamma_{yyyy}^{y_0}$,$\gamma_{yyyy}^{y_1}$,$\gamma_{yyyy}^{\mathrm{rest}}(\equiv \gamma_{yyyy} - \gamma_{yyyy}^{y_0} - \gamma_{yyyy}^{y_1})$] (×$10^3$ a.u.) of PAH[6,7] calculated by the LC-UBLYP/6-31G* method

	NSP	SP
y_0	1.00	1.00
y_1	0.75	0.52
$\gamma_{yyyy}^{y_0}$	−3 (∼0%)	−3 (∼0%)
$\gamma_{yyyy}^{y_1}$	153 (15%)	327 (30%)
$\gamma_{yyyy}^{\mathrm{rest}}$	854 (85%)	779 (70%)
γ_{yyyy}	1,004	1,103

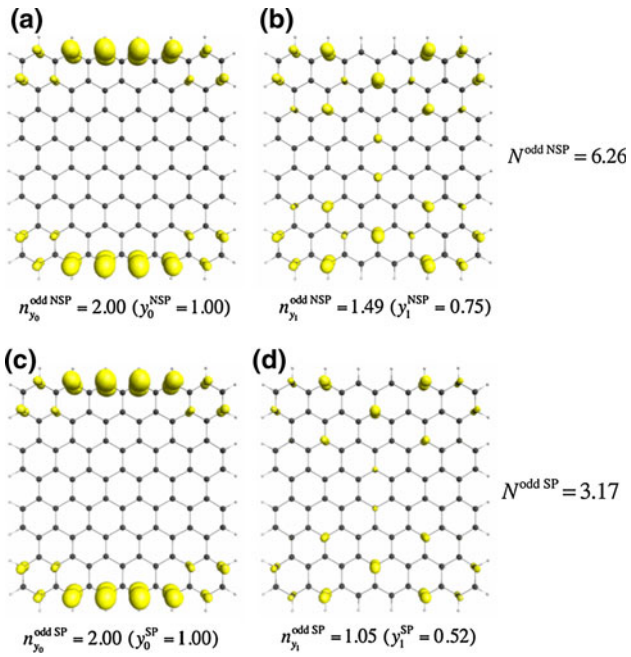

Fig. 6 Non-spin projected and spin projected odd electron densities [$D^{y_i\mathrm{NSP}}(\boldsymbol{r})$, $D^{y_i\,\mathrm{SP}}(\boldsymbol{r})$] as well as odd electron numbers $\left(n_{y_i}^{\mathrm{odd\,NSP}}, n_{y_i}^{\mathrm{odd\,SP}}\right)$ corresponding to the diradical characters y_0^{NSP} (**a**), y_1^{NSP} (**b**), y_0^{SP} (**c**) and y_1^{SP} (**d**) of PAH[6,7] calculated by the LC-UBLYP/6-31G* method. The yellow surfaces represent densities with iso-surfaces of 0.0025 a.u. Total odd electron numbers N^{oddNSP} and N^{oddSP} are also shown

Next, we address the spin projection effects (Table 2), carried out using Eqs. 21 and 22 on the occupation numbers of the HONO − i and LUNO + i with i = 0–69. This provides a converged γ_{yyyy} value around $i_{\max} = 30$, but the convergence is slightly slower than in the case of PAH[3,3] (Fig. 5). Moreover, the enhancement ratio of $\gamma_{yyyy}^{\mathrm{SP}}$ with respect to $\gamma_{yyyy}^{\mathrm{NSP}}$ is the largest at $i_{\max} = 1$ (17% at $i_{\max} = 1$) after removal of the spin contamination effects associated with the pair of NOs with intermediate y_i. Then, successive SP corrections reduce γ_{yyyy} so that at $i_{\max} = 69$, it is only 10% larger than the NSP value. In parallel, the y_1 value decreases by 31% (0.75 → 0.52), but the y_0 value (∼1) is almost unchanged as seen from Eqs. 21 and 22. Accordingly, the amplitude of $D^{y_1\,\mathrm{SP}}(\boldsymbol{r})$ $\left[n_{y_1}^{\mathrm{odd\,SP}}\left(\equiv n_{\mathrm{HONO-1}}^{\mathrm{odd\,SP}} + n_{\mathrm{LUNO+1}}^{\mathrm{odd\,SP}}\right) = 1.05\right]$ is reduced—but the distribution pattern is the same—(Fig. 6b and d), while that of $D^{y_0\,\mathrm{SP}}(\boldsymbol{r})$ $n_{y_0}^{\mathrm{oddSP}} = 2.00$ is unchanged (Fig. 6a and c). The total odd electron number is then reduced from 6.26 (NSP) to 3.17 (SP), which confirms that PAH[6,7] should be regarded as a tetra-radical singlet system with an

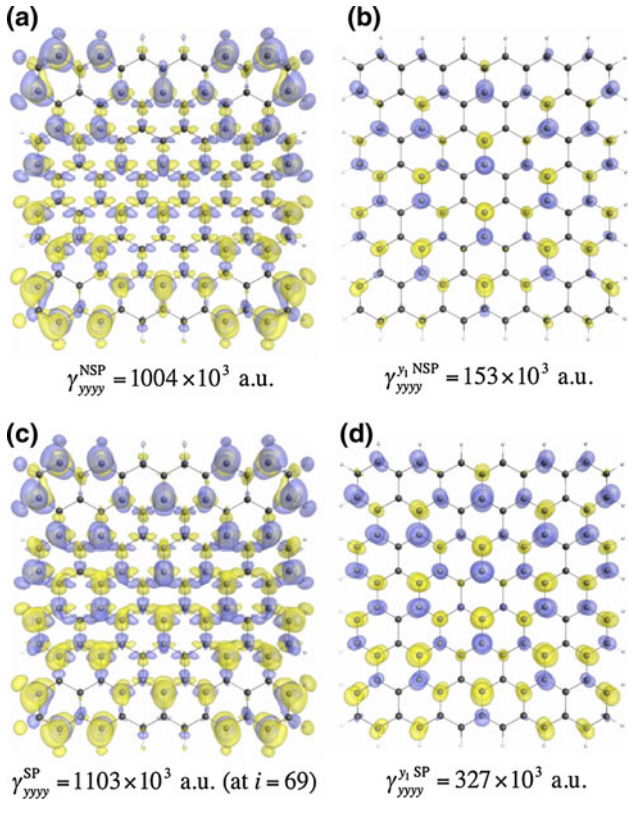

Fig. 7 Non-spin projected and spin projected γ_{yyyy} [γ_{yyyy}^{NSP} (**a**), $\gamma_{yyyy}^{y_1\,NSP}$ (**b**), γ_{yyyy}^{SP} (at $i = 69$) (**c**), $\gamma_{yyyy}^{y_1\,SP}$ (**d**)] density distributions of PAH[6,7] calculated by the LC-UBLYP/6-31G* method. The yellow and blue meshes represent positive and negative densities with iso-surface ±300 a.u., respectively

intermediate y_1 value. Such reductions in the successive diradical characters and the odd electron densities are caused by removing the contamination of higher spin components. In contrast, the spin projection effects increase the γ_{yyyy} amplitude by only 10%. This results from a partial cancelation between the increase related to the spin projection of $n_{\text{HONO-1}}$ and the decrease associated with the subsequent ones. Thus, the contribution of $\gamma_{yyyy}^{y_1}$ to the total γ_{yyyy} increases from 15 to 30%, while the remaining contribution decreases from 85 to 70% upon spin projection. Figure 7c and d shows the γ_{yyyy}^{SP} and $\gamma_{yyyy}^{y_1\,SP}$ density distributions, respectively. As expected from the comparison between the spin projected and non-spin projected $\gamma_{yyyy}^{y_1}$ and γ_{yyyy} values, the amplitudes and distribution patterns of the γ_{yyyy}^{SP} and γ_{yyyy}^{NSP} densities are similar, while the $\gamma_{yyyy}^{y_1}$ density is significantly enhanced upon SP, in particular, on the four-corner phenalenyl blocks and on the y-symmetry axis, providing a better match with the total γ_{yyyy}^{SP} density.

Note that the relatively small influence of spin projection effects on γ for PAH[3] and PAH[6,7] can be related to their intermediate or large diradical character, as illustrated by the results on the 1,3-dipoles (see Fig. 1). Indeed, using the UHF NO occupation numbers [20] $y_0 = 0.510$ for PAH[3,3] and $(y_0, y_1) = (1.000, 0.763)$ for PAH[6,7].

4 Extension to dynamic odd electron and (hyper)polarizability densities

This section is devoted to the extension of the method to the dynamic case, where the density matrix of a system evolves under external time-dependent fields $\boldsymbol{F}(t)$ (e.g., $\boldsymbol{F}(t) = \boldsymbol{F}\cos\omega t$ for the one-mode case). A corresponding electronic Hamiltonian H for N-electron system reads

$$H = -\frac{1}{2}\sum_{i=1}^{N}\nabla_i^2 - \sum_{i=1}^{N}\sum_{X}\frac{Z_X}{r_{iX}} + \sum_{i=1}^{N}\sum_{j>i}^{N}\frac{1}{r_{ij}} + \sum_{i=1}^{N}\boldsymbol{F}(t)\cdot\boldsymbol{r}_i, \tag{24}$$

which induces a dynamic electric polarization $\boldsymbol{p}(t)$ in the molecule. First, the dynamic odd electron density is defined in a similar way to the static case. This quantity enables us to analyze the spatio-temporal behavior of the odd electrons in each NO. It is noted that the partition to y_i is impossible in general because the time-dependent wave function involves various types of excited determinants (in addition to perfect-pairing double excitations) as a result of the external fields, preventing us from defining y_i based on the occupation numbers of HONO-i and LUNO + i pairs since $n_{\text{HONO}-i}(t) + n_{\text{LUNO}+i}(t) \neq 2$. This also implies that the perfect-pairing spin projection scheme (Eq. 21) cannot be applied to the dynamic case. Alternatively, we can obtain the time-evolution of the odd electron densities $[D_k(\boldsymbol{r},t)]$ and odd electron numbers $[n_k^{\text{odd}}(t)]$ by using the time-dependent NOs $\{\phi_k(\boldsymbol{r},t)\}$ and occupation numbers $\{n_k(\boldsymbol{r},t)\}$:

$$D_k(\boldsymbol{r},t) = \min[2 - n_k(t), n_k(t)]\phi_k^*(\boldsymbol{r},t)\phi_k(\boldsymbol{r},t), \tag{25}$$

and

$$n_k^{\text{odd}}(t) = \text{Tr}D_k(\boldsymbol{r},t) = \min[2 - n_k(t), n_k(t)]. \tag{26}$$

The time-dependent NOs and occupation numbers are obtained from the diagonalization of the time-dependent one-electron reduced density matrix:

$$d_{lm}(t) \equiv \iint \phi_l^*(\boldsymbol{r}, t=0)d(\boldsymbol{r},\boldsymbol{r}';t)\phi_m(\boldsymbol{r}', t=0)d\boldsymbol{r}d\boldsymbol{r}', \tag{27}$$

where this quantity is complex in general, $\{\phi_l(\boldsymbol{r}, t=0)\}$ is the NO basis at $t = 0$, and $d(\boldsymbol{r},\boldsymbol{r}';t)$ is the one-electron reduced density matrix at time t. The time-dependent total odd electron density and number are then defined by

$$D(\boldsymbol{r},t)=\sum_{k=1}^{M}D_k(\boldsymbol{r},t),$$

and

$$N^{\mathrm{odd}}(t)=\sum_{k=1}^{M}n_k^{\mathrm{odd}}(t)\quad[N^{\mathrm{odd}}(t)\le N] \tag{28}$$

These quantities are measures of the time-evolution of the open-shell character. Next, we define the dynamic (hyper) polarizability density [90] based on the time-dependent one-electron reduced density:

$$d(\boldsymbol{r},t)=\sum_{k=1}^{M}n_k(t)\phi_k^*(\boldsymbol{r},t)\phi_k(\boldsymbol{r},t)\equiv\sum_{k=1}^{M}d_k(\boldsymbol{r},t) \tag{29}$$

After taking the Fourier transformation of the previous equation, the relationships between the dynamic (hyper) polarizabilities and their densities are obtained

$$\begin{aligned}\alpha_{ab}(-\omega;\omega)&=-\int r_a d_b^{\alpha}(\boldsymbol{r},\omega)d\boldsymbol{r}\\&=\sum_{k=1}^{M}\left(-\int r_a d_b^{\alpha k}(\boldsymbol{r},\omega)d\boldsymbol{r}\right)\equiv\sum_{k=1}^{M}\alpha_{ab}^{k}(-\omega;\omega),\end{aligned} \tag{30}$$

$$\begin{aligned}\beta_{abc}(-2\omega;\omega,\omega)&=-\frac{1}{2!}\int r_a d_{bc}^{\beta(\mathrm{SHG})}(\boldsymbol{r},2\omega)d\boldsymbol{r}\\&=\sum_{k=1}^{M}\left(-\frac{1}{2!}\int r_a d_{bc}^{\beta(\mathrm{SHG})k}(\boldsymbol{r},2\omega)d\boldsymbol{r}\right)\\&\equiv\sum_{k=1}^{M}\beta_{abc}^{k}(-2\omega;\omega,\omega),\end{aligned} \tag{31}$$

and

$$\begin{aligned}\gamma_{abcd}(-3\omega;\omega,\omega,\omega)&=-\frac{1}{3!}\int r_a d_{bcd}^{\gamma(\mathrm{THG})}(\boldsymbol{r},3\omega)d\boldsymbol{r}\\&=\sum_{k=1}^{M}\left(-\frac{1}{3!}\int r_a d_{bcd}^{\gamma(\mathrm{THG})k}(\boldsymbol{r},3\omega)d\boldsymbol{r}\right)\\&\equiv\sum_{k=1}^{M}\gamma_{abcd}^{k}(-3\omega;\omega,\omega,\omega).\end{aligned} \tag{32}$$

Here, $d_b^{\alpha}(\boldsymbol{r},\omega)$, $d_{bc}^{\beta(\mathrm{SHG})}(\boldsymbol{r},2\omega)$ and $d_{bcd}^{\gamma(\mathrm{THG})}(\boldsymbol{r},3\omega)$ represent the dynamic (hyper)polarizability densities, while $d_b^{\alpha k}(\boldsymbol{r},\omega), d_{bc}^{\beta(\mathrm{SHG})k}(\boldsymbol{r},2\omega), d_{bcd}^{\gamma(\mathrm{THG})k}(\boldsymbol{r},3\omega)$ are the contributions from the kth NO. For example, the diagonal tensor components of the latter are given by

$$d_b^{\alpha k}(\boldsymbol{r},\omega)\equiv\frac{d^k(\boldsymbol{r},\omega)}{\varepsilon_b(\omega)}, \tag{33}$$

$$d_{bb}^{\beta(\mathrm{SHG})k}(\boldsymbol{r},2\omega)\equiv\frac{d^k(\boldsymbol{r},2\omega)}{2\varepsilon_b^2(\omega)}, \tag{34}$$

and

$$d_{bbb}^{\gamma(\mathrm{THG})k}(\boldsymbol{r},3\omega)\equiv\frac{2}{9}\frac{d^k(\boldsymbol{r},3\omega)}{\varepsilon_b^3(\omega)}. \tag{35}$$

Here, ε is the field amplitude in the one-frequency $\varepsilon(e^{-i\omega t}+e^{i\omega t})$ term, so that $F=2\varepsilon$, where F is the field amplitude in the $F\cos\omega t$ term used in Eq. 24. The dynamic β and γ densities have different numerical coefficients from those in our previous paper [90] in order to be consistent with the static (hyper)polarizability densities defined in Eqs. 13 and 14. Details on the derivations and on the extension to other NLO processes have been presented in our previous papers [90–92].

Although no results are presented here, it is important to discuss briefly the applicability of time-dependent (TD) DFT methods for the calculation of these time-dependent properties in open-shell molecular systems. Though the TDDFT scheme using appropriate exchange–correlation functionals, e.g., LC-UBLYP and CAM-B3LYP [93] functionals, can generally well reproduce the excitation energies and transition properties for closed-shell molecules, the applicability of TDUDFT to open-shell systems has not yet been elucidated in details. Moreover, for dynamic high-order responses such as γ, the multiple-electron excitation contributions are essential, even for a qualitative description of the high-lying excited states involved in the associated virtual excitation processes. These properties will be reproduced well by the complete active space (CAS)-DFT method [94–104], which provides a balanced description of non-dynamical and dynamical correlations by combining a multi-reference wave function method with a DFT correlation functional though it is still difficult to apply it to large-size systems. Therefore, the development of appropriate TDDFT methods to predict these properties for large-size open-shell systems is certainly one of the most challenging problems.

5 Concluding remarks

The (hyper)polarizabilities and their densities have been re-expressed based on the natural orbitals and occupation numbers as well as on the diradical characters defined by the odd electron density. In the spin-unrestricted single-determinant case, the static (hyper)polarizabilities and their densities are partitionable into the contributions corresponding to each diradical character. This method is then applicable to multi-radical systems and enables us to investigate the contribution of each odd electron pair to the (hyper)polarizability. Then, within the spin-unrestricted single-determinantal frame, an approximate spin projected (SP) scheme has been developed to improve the description of the odd electron density and of the (hyper)polarizabilities. It is based on a correction of the occupation numbers.

In order to assess the performance of the present method of calculation, we have compared the second hyperpolarizabilities of typical diradical 1,3-dipole systems, calculated using the present SP-LC-UBLYP/UBPW91 scheme to those evaluated with the UCCSD(T) method. The SP method semi-quantitatively reproduces the UCCSD(T) results, in particular by correcting the overshot γ values in the small diradical character region that are obtained using the corresponding non-spin projected approaches. We have also demonstrated that the partitioned odd electron densities of rectangular graphene nanoflakes, PAH[3,3] and PAH[6,7], can help clarify the spatial contributions of the odd electrons to the di-, tetra-, …, multi-radical characters and subsequently to the (hyper)polarizabilities. The impact of spin projections has also been addressed.

Furthermore, we presented a generalization of the method to the dynamic (hyper)polarizabilities and their densities, including the investigation of the dynamic odd electron density, which is a measure of the time-evolution of the open-shell characters of multi-radical systems under time-dependent external electric fields.

In summary, the present method of analysis provides intuitive and pictorial descriptions of the static and dynamic (non)linear response properties in connection with the spatial distributions of the odd electrons and with the diradical characters for open-shell molecules including delocalized multi-radical systems. This method is applicable to arbitrary systems, e.g., large-size open-shell molecular and aggregate systems in both gas and condensed phases. Based on related investigations on the hyperpolarizabilities of extended systems, the reliability of SP-UDFT results is predicted to depend on the exchange–correlation functionals, and therefore, long-range corrected exchange–correlation functionals are better suited than more conventional functionals.

Acknowledgments This work was supported by Grant-in-Aid for Scientific Research (Nos. 21350011 and 20655003) and "Japan-Belgium Cooperative Program" (J091102006) from Japan Society for the Promotion of Science (JSPS), and the global COE (center of excellence) program "Global Education and Research Center for Bio-Environmental Chemistry" of Osaka University. Theoretical calculations were partly performed using Research Center for Computational Science, Okazaki, Japan. E.B. thanks the Interuniversity Attraction Pole on "Functional Supramolecular Systems" (IUAP No. P6-27) for her postdoctoral grant. This work has also been supported by the Academy Louvain (ARC "Extended-π-Conjugated Molecular Tinkertoys for Optoelectronics, and Spintronics") and by the Belgian Government (IUAP No P06-27 "Functional Supramolecular Systems").

References

1. Salem L, Rowland C (1972) Angew Chem Int Ed 11:92
2. Borden WT (ed) (1982) Diradicals. Wiley-Interscience, New York
3. Rajca A (1994) Chem Rev 94:871
4. Klessinger M, Michl J (1995) Excited states and photo-chemistry of organic molecules, revised and improved english-language edition. Wiley-VCH, New York
5. Borden WT, Davidson ER (1977) J Am Chem Soc 99:4587
6. Adam W, Borden WT, Burda C, Foster H, Heidenfelder T, Heubes M, Hrovat DA, Kita F, Lewis SB, Scheutzow D, Wirz J (1998) J Am Cem Soc 120:593
7. Staroverov VN, Davidson ER (2000) J Am Chem Soc 122:186
8. Abe M, Adam W, Hara M, Hattori M, Majima T, Nojima M, Tachibana K, Tojo S (2002) J Am Chem Soc 124:6540
9. Jung Y, Head-Gordon M (2003) Chem Phys Chem 4:522
10. Scheschkewitz D, Amii H, Gomitzka H, Schoeller WW, Bourissou D, Bertrand G (2002) Science 295:1880
11. Cui C, Brynda M, Olmstead MM, Power PP (2004) J Am Chem Soc 126:6510
12. Paci I, Johnson JC, Chen X, Rana G, Popovic D, David DE, Nozik AJ, Ratner MA, Michl J (2006) J Am Chem Soc 128:16546
13. Suaud N, Bonnet ML, Boilleau C, Labéguerie P, Guihéry N (2009) J Am Chem Soc 131:715
14. Houk KN, Lee PS, Nendel M (2001) J Org Chem 66:5517
15. Bendikov M, Duong HM, Starkey K, Houk KN, Carter EA, Wudl F (2004) J Am Chem Soc 126:7416
16. Chen Z, Jiang D, Lu X, Bettinger HF, Dai S, PvR Schleyer, Houk KN (2007) Org Lett 9:5449
17. Hachmann J, Dorando JJ, Avilés M, Chan GK-L (2007) J Chem Phys 127:134309
18. Jiang D, Dai S (2008) J Phys Chem A 112:332
19. Tönshoff C, Bettinger HF (2010) Angew Chem Int Ed 49:4125. doi:10.1002/anie.200906355
20. Nagai H, Nakano M, Yoneda K, Kishi R, Takahashi H, Shimizu A, Kubo T, Kamada K, Ohta K, Botek E, Chanpagne B (2010) Chem Phys Lett 489:212
21. Trinquier G, Suaud, N, Malrieu JP (2010) Chem Eur J 16:8762
22. Wang WL, Meng S, Kaxiras E (2008) Nano Lett 8:241
23. Yazyev OV, Wang WL, Meng S, Kaxiras E (2008) Nano Lett 8:766
24. Ezawa M (2007) Phys Rev B 76:245415
25. Vandeschuren M, Hermet P, Meunier V, Henrard L, Lambin Ph (2008) Phys Rev B 78:195401
26. F-Rossier J, Palacios JJ (2007) Phys Rev Lett 99:177204
27. Dias JR (2008) Chem Phys Lett 467:200
28. Son Y-W, Cohen ML, Louie SG (2006) Nature 444:347
29. Kubo T, Shimizu A, Sakamoto M, Uruichi M, Yakushi K, Nakano M, Shiomi D, Sato K, Takui T, Morita Y, Nakasuji K (2005) Angew Chem Int Ed 44:6564
30. Konishi A, Hirao Y, Nakano M, Shimizu A, Botek E, Champagne B, Shiomi D, Sato K, Takui T, Matsumoto K, Kurata H, Kubo T (2010) J Am Chem Soc 132:11021
31. Lahti PM, Ichimura AS, Sanborn JA (2001) J Phys Chem A 105:251
32. Serwinski PR, Lahti PM (2003) Org Lett 5:2099
33. Ito A, Urabe M, Tanaka K (2007) Angew Chem Int Ed 46:3300
34. Matsuda K, Irie M (2001) Chem Eur J 7:3466
35. Rajca A, Shiraishi K, Pink M, Rajca S (2007) J Am Chem Soc 129:7232
36. Rajca A, Vale M, Rajca S (2008) J Am Chem Soc 130:9099
37. Train C, Norel L, Baumgarten M (2009) Coord Chem Rev 253:2342
38. Shimizu A, Uruichi M, Yakushi K, Matsuzaki H, Okamoto H, Nakano M, Hirao Y, Matsumoto K, Kurata H, Kubo T (2009) Angew Chem Int Ed 48:5482
39. Huang J, Kertesz M (2007) J Am Chem Soc 129:1634
40. Tian YH, Kertesz M (2010) J Am Chem Soc 132:10648

41. Yamaguchi K (1990) In: Carbo R, Klobukowski M (eds) Self-consistent field: theory and applications. Elsevier, Amsterdam, p 727
42. Nakano M, Kishi R, Nitta T, Kubo T, Nakasuji K, Kamada K, Ohta K, Champagne B, Botek E, Yamaguchi K (2005) J Phys Chem A 109:885
43. Nakano M, Kishi R, Ohta S, Takebe A, Takahashi H, Furukawa S, Kubo T, Morita Y, Nakasuji K, Yamaguchi K, Kamada K, Ohta K, Champagne B, Botek E (2006) J Chem Phys 125:74113
44. Nakano M, Kishi R, Ohta S, Takahashi H, Kubo T, Kamada K, Ohta K, Botek E, Champagne B (2007) Phys Rev Lett 99:033001
45. Nakano M, Kubo T, Kamada K, Ohta K, Kishi R, Ohta S, Nakagawa N, Takahashi H, Furukawa S, Morita Y, Nakasuji K (2006) Chem Phys Lett 418:142
46. Ohta S, Nakano M, Kubo T, Morita Y, Nakasuji K, Ohta S, Nakano M, Kubo T, Kamada K, Ohta K, Kishi R, Nakagawa N, Champagne B, Botek E, Takebe A, Umezaki S, Nate M, Takahashi H, Furukawa S, Morita Y, Nakasuji K, Yamaguchi K (2007) J Phys Chem A 111:3633
47. Fukui H, Kishi R, Minami T, Nagai H, Takahashi H, Kubo T, Kamada K, Ohta K, Champagne B, Botek B, Nakano M (2008) J Phys Chem A 112:8423
48. Serrano-Andrés L, Avramopoulos A, Li J, Labéguerie P, Bégué D, Kellö V, Papadopoulos MG (2009) J Chem Phys 131:134312
49. Nakano M, Nagai H, Fukui H, Yoneda K, Kishi R, Takahashi T, Shimizu A, Kubo T, Kamada K, Ohta K, Champagne B, Botek B (2008) Chem Phys Lett 467:120
50. Kamada K, Ohta K, Kubo T, Shimizu A, Morita Y, Nakasuji K, Kishi R, Ohta S, Furukawa S, Takahashi H, Botek E, Champagne B, Nakano M (2007) Angew Chem Int Ed 46:3544
51. Nakano M, Yoneda K, Kishi R, Takahashi T, Kubo T, Kamada K, Ohta K, Botek E, Champagne B (2009) J Chem Phys 131:114316
52. Nakano M, Shigemoto I, Yamada S, Yamaguchi K (1995) J Chem Phys 103:4175
53. Jha PC, Rinkevicius Z, Ågren H (2009) ChemPhysChem 10:817
54. Li ZJ, Wang FF, Li ZR, Xu HL, Huang XR, Wu D, Chen W, Yu GT, Gu FL, Aoki Y (2009) Phys Chem Chem Phys 11:402
55. Takatsuka K, Fueno T, Yamaguchi K (1978) Theor Chim Acta 48:175
56. Staroverov VN, Davidson E (2000) Chem Phys Lett 330:161
57. Head-Gordon M (2003) Chem Phys Lett 372:508
58. Yamanaka S, Okumura M, Nakano M, Yamaguchi K (1994) J Mol Structure (Theochem) 310:205
59. Kitagawa Y, Saito T, Nakanishi Y, Kataoka Y, Matsui T, Kawakami T, Okumura M, Yamaguchi K (2009) J Phys Chem A 113:15041
60. Yamaguchi K (1975) Chem Phys Lett 33:330
61. Kishi R, Bonness S, Yoneda K, Takahashi H, Nakano M, Botek E, Champagne B, Kubo T, Kamada K, Ohta K, Tsuneda T (2010) J Chem Phys 132:094107
62. Stoll H, Savin A (1985) In: Dreizler R, da Providencia J (eds) Density Functional Methods in Physics, Plenum, New York, p 177
63. Leininger T, Stoll H, Werner H-J, Savin A (1997) Chem Phys Lett 275:151
64. Iikura H, Tsuneda T, Yanai T, Hirao K (2001) J Chem Phys 115:3540
65. Tawada Y, Tsuneda T, Yanigasawa S, Yanai T, Hirao K (2004) J Chem Phys 120:8425
66. Hunt KLC (1984) J Chem Phys 80:393
67. Hunt KLC (1995) J Chem Phys 103:3552
68. Tisko EL, Li X, Hunt KLC (1995) J Chem Phys 103:6873
69. Geskin VM, Brédas JL (1998) J Chem Phys 109:6163
70. Leclercq A, Zojer E, Jang SH, Barlow S, Geskin V, Jen AKY, Marder SR, Brédas JL (2006) J Chem Phys 124:044510
71. Ye A, Autschbach J (2006) J Chem Phys 124:234101
72. Krylov AI (2001) Chem Phys Lett 338:375
73. Krylov AI (2001) Chem Phys Lett 350:522
74. Sekino H, Bartlett RJ (1993) J Chem Phys 98:3022
75. Nakano M, Kishi R, Nakagawa N, Ohta S, Takahashi H, Furukawa S, Kamada K, Ohta K, Champagne B, Botek E, Yamada S, Yamaguchi K (2006) J Phys. Chem A 110:4238
76. Champagne B, Botek B, Nakano M, Nitta T, Yamaguchi K (2005) J Chem Phys 122:114315
77. Champagne B, Perpète EA, van Gisbergen SJA, Baerends EJ, Soubra-Ghaoui C, Robins KA, Kirtman B (1998) J Chem Phys 109:10489 Erratum (1999) 110:11664
78. Champagne B, Perpète EA, Jacquemin D, van Gisbergen SJA, Baerends EJ, Soubra-Ghaoui C (2000) J Phys Chem A 104:4755
79. van Gisbergen SJA, Schipper PRT, Gritsenko OV, Baerends EJ, Snijders JG, Champagne B, Kirtman B (1999) Phys Rev Lett 83:694
80. Kummel S, Kronik L, Perdew JP (2004) Phys Rev Lett 93:213002
81. Mori-Sanchez P, Wu Q, Yang W (2003) J Chem Phys 119:11031
82. Sekino H, Maeda Y, Kamiya M, Hirao K (2007) J Chem Phys 126:014107
83. Kirtman B, Bonness S, Ramirez-Solis A, Champagne B, Matsumoto H, Sekino H (2008) J Chem Phys 128:114108
84. Bonness S, Fukui H, Yoneda K, Kishi R, Champagne B, Botek E, Nakano M (2010) Chem Phys Lett 493:195
85. Nakano M, Takebe A, Kishi R, Ohta S, Nate M, Kubo T, Kamada K, Ohta K, Champagne B, Botek E, Takahashi H, Furukawa S, Morita S, Nakasuji K (2006) Chem Phys Lett 432:473
86. Song J-W, Hirosawa T, Tsuneda T, Hirao K (2007) J Chem Phys 126:154105
87. Frisch MJ, Trucks GW, Schlegel HB, Scuseria GE, Robb MA, Cheeseman JR, Scalmani G, Barone V, Mennucci B, Petersson GA, Nakatsuji H, Caricato M, Li X, Hratchian HP, Izmaylov AF, Bloino J, Zheng G, Sonnenberg JL, Hada M, Ehara M, Toyota K, Fukuda R, Hasegawa J, Ishida M, Nakajima T, Honda Y, Kitao O, Nakai H, Vreven T, Montgomery JA Jr, Peralta JE, Ogliaro F, Bearpark M, Heyd JJ, Brothers E, Kudin KN, Staroverov VN, Kobayashi R, Normand J, Raghavachari K, Rendell A, Burant JC, Iyengar SS, Tomasi J, Cossi M, Rega N, Millam NJ, Klene M, Knox JE, Cross JB, Bakken V, Adamo C, Jaramillo J, Gomperts R, Stratmann RE, Yazyev O, Austin AJ, Cammi R, Pomelli C, Ochterski JW, Martin RL, Morokuma K, Zakrzewski VG, Voth GA, Salvador P, Dannenberg JJ, Dapprich S, Daniels AD, Farkas Ö, Foresman JB, Ortiz JV, Cioslowski J, Fox DJ (2009) Gaussian 09, Revision A.1. Gaussian, Inc., Wallingford CT
88. Filatov M, Cremer D (2005) J Chem Phys 123:124101
89. Nakano M, Yamada S, Shigemoto I, Yamaguchi K (1996) Chem Phys Lett 250:247
90. Nakano M, Yamaguchi K (1994) Phys Rev A 50:2989
91. Nakano M, Yamaguchi K, Matsuzaki Y, Tanaka K, Yamabe T (1995) J Chem Phys 102:2986
92. Yanai T, Tew DP, Handy NC (2004) Chem Phys Lett 393:51
93. Savin A, Flad HJ (1995) Int J Quantum Chem 56:327
94. Gori-Giorgi P, Savin A (2006) Phys Rev A 73:3250
95. Fromager E, Toulouse J, Jensen HJA (2007) J Chem Phys 126:074111
96. Kusakabe K (2001) J Phys Soc Jpn 70:2038
97. Yamanaka S, Nakata K, Takada T, Kusakabe K, Ugalde JM, Yamaguchi K (2006) Chem Lett 35:242

98. Yamanaka S, Nakata K, Ukai T, Takada T, Yamaguchi K (2006) Int J Quantum Chem 16:3312
99. Miehlich B, Stoll H, Savin A (1997) Mol Phys 91:527
100. Gräfenstein J, Cremer D (2000) Chem Phys Lett 316:569
101. Gusarov S, Malmqvist PÅ, Lindh R, Roos BO (2004) Theor Chem Acc 112:84
102. Pérez-Jiménez AJ, Pérez-Jord JM (2007) Phys Rev A 75:012503
103. Takeda R, Yamanaka S, Yamaguchi K (2002) Chem Phys Lett 366:321
104. Takeda R, Yamanaka S, Yamaguchi K (2004) Int J Quantum Chem 96:463